City Research Online

City St George's, University of London

Citation: Aqel, O., White, M. & Sayma, A. I. (2021). Binary interaction uncertainty in the optimisation of a transcritical cycle: Consequences on cycle and turbine design. Paper presented at the 4th European sCO2 Conference for Energy Systems, 23-24 Mar 2021, Online. doi: 10.17185/duepublico/73959

This is the published version of the paper.

This version of the publication may differ from the final published version. To cite this item please consult the publisher's version.

Permanent repository link: https://openaccess.city.ac.uk/id/eprint/25856/

Link to published version: https://doi.org/10.17185/duepublico/73959

Copyright and Reuse: Copyright and Moral Rights remain with the author(s) and/or copyright holders. Copies of full items can be used for personal research or study, educational, or not-for-profit purposes without prior permission or charge, unless otherwise indicated, provided that the authors, title and full bibliographic details are credited, a hyperlink and/or URL is given for the original metadata page and the content is not changed in any way. For full details of reuse please refer to City Research Online policy.

City Research Online: http://openaccess.city.ac.uk/ publications@citystgeorges.ac.uk

The 4th European sCO2 Conference for Energy Systems
March 23-24, 2021, Online Conference

2021-sCO2.eu-126

BINARY INTERACTION UNCERTAINTY IN THE OPTIMISATION OF A TRANSCRITICAL CYCLE: CONSEQUENCES ON CYCLE AND TURBINE DESIGN

Omar Aqel*
Department of Mechanical Engineering and Aeronautics, City University of London
London, UK
Email: Omar.Aqel@city.ac.uk

Martin White
Department of Mechanical Engineering and Aeronautics, City University of London
London, UK
Email: Martin.White@city.ac.uk

Abdulnaser Sayma
Department of Mechanical Engineering and Aeronautics, City University of London
London, UK
Email: A.Sayma@city.ac.uk

ABSTRACT

Doping CO_2 with an additional fluid to produce a CO_2-based mixture is predicted to enhance the performance of the super critical CO_2 power cycle and lower its cost when adapted to Concentrated Solar Power plants. A consistent fluid mixture modelling process is necessary to reliably design and predict the performance of turbines operating with CO_2-based working fluids. This paper aims to quantify the significance of the choice of an Equation of State (EoS) and the uncertainty in the binary interaction parameter (k_{ij}) on the cycle and turbine design.

To evaluate the influence of the thermodynamic model, an optimisation study of a 100 MW_e simple recuperated transcritical CO_2 cycle is conducted for a combination of three mixtures, four equations of state, and three possible values of the binary interaction parameter. Corresponding multi-stage axial turbines are then designed and compared based on the optimal cycle conditions.

Results show that the choice of the dopant fraction which yields maximum cycle thermal efficiency is independent from the fluid model used. However, the predicted thermal efficiency of the mixtures is reliant on the fluid model. Absolute thermal efficiency may vary by a maximum of 1% due to the choice of the EoS, and by up to 2% due to k_{ij} uncertainty. The maximum difference in the turbine geometry due to EoS selection corresponded to a 6.3% (6.6 cm) difference in the mean diameter and a 18.8% (1.04 cm) difference in the blade height of the final stage. On the other hand, the maximum difference in turbine geometry because of k_{ij} uncertainty amounted to 6.7% (5.6 cm) in mean diameter and 27.3% (2.73 cm) in blade height of the last stage.

INTRODUCTION

Several studies have identified the potential of supercritical carbon dioxide (sCO_2) cycles to outperform traditional steam cycles in concentrated solar power (CSP) plants [1]–[6]. However, the lack of cooling water hinders the performance of CSP plants and reduces its thermal efficiency. This is because the use of air-cooled condensers prevents condensing cycles, increases the cycle's compression work, and limits its efficiency.

Doping CO_2 with an additional fluid to produce a CO_2-based mixture could alleviate the limitations of dry cooling. It does so by increasing the critical temperature of the working fluid and expanding the operation of transcritical carbon dioxide (tCO_2) cycles, which compress the fluid in its liquid state and expand it in its supercritical state, into arid environments [7].

A variety of dopants have been considered in the past. Xia et al. [8] identified organic dopants that might improve cycle thermal efficiency. However, Invernizzi et al. [9] concluded that organic dopants, such as hydrocarbon mixtures, are not stable enough for temperatures above 400 ℃, which is below the expected temperature range of CSP, and hence alternatives are needed.

Inorganic dopants with critical temperatures higher than that of CO_2, such as dinitrogen tetroxide (N_2O_4) or titanium tetrachloride ($TiCl_4$), were proposed by Bonalumi et al. [10] and further studied by Manzolini et al. [11]. Results showed that they may achieve cycle efficiencies of up to 50%, reduce the specific

* corresponding author(s)
Email address: Omar.Aqel@city.ac.uk

DOI: 10.17185/duepublico/73959

cost of the power block by 50%, and reduce the levelised cost of electricity (LCoE) by 11 to 13% with respect to a conventional steam cycle. Moreover, the power block cost may be reduced by 20% compared to pure sCO_2.

Regardless of the working fluid, the choice of the thermodynamic equation that describes the fluid's state properties (fluid model) affects cycle performance prediction and equipment sizing. Specifically, the thermodynamic properties determine the cycle thermal efficiency and equipment sizing, while the transport properties affect equipment sizing. However, transport properties are not considered in this study because they are not directly calculated by an equation of state (EoS). It is also worth noting that the choice of the fluid model does not alter the actual behavior of the fluid or the cycle, but only effects the ability to predict their behavior.

The influence of the fluid model on the estimated cycle performance and equipment sizing has been investigated in the past. Zhao et al. [12] conducted a selection procedure which compared six EoS to identify the best option for the modelling of a pure CO_2 working fluid in a recompression cycle. The six EoS compared were of three types: (1) Cubic-type, including the Peng-Robinson (PR), the Peng-Robinson combined with Boston-Mathias alpha function (PR-BM), and the Soave-Redlich-Kwong (SRK); (2) Virial-type, including the Lee-Kesler-Plocker (LKP) and the Benedict-Webb-Rubin modified by Starling and Nishiumi (BWRS); and (3) Helmholtz-type in the form of the Span-Wagner (SW) EoS. It was concluded that the SW EoS provided the most accurate predictions of CO_2 properties in the near-critical and supercritical regions.

In the study by Zhao et al. [12], the Mean Absolute Percentage Error (MAPE) in the specific heat calculated by SW EoS was 0.5% compared to experimental data. Other EoS resulted in MAPE of about 2% in the calculated specific heat values. At most the variation in thermal efficiency was within 2% depending on the EoS. In terms of equipment sizing, they noted that a deviation of 10% in recuperator size (specified by the product of the overall heat transfer coefficient U and heat exchange area A) and compressor diameter is possible depending on the choice of EoS. The variation in the compressor size was attributed to its operation near the critical point where evaluation of the specific heat capacity becomes less precise. Conversely, the influence on turbine diameter was found to be more limited (from 0.2% to 3.0%), which is expected since equations of state converge to the ideal gas law at high temperatures above the critical dense-gas region.

The study of mixtures adds another uncertainty in thermodynamic property predictions because of the use of the Binary Interaction Parameter (k_{ij}), which is a correction factor applied to an EoS to account for intermolecular interactions between mixture components. A value for k_{ij} may be obtained by regressions based on experimental Vapor-Liquid Equilibrium (VLE) data, where k_{ij} is calibrated to fit the EoS predictions with empirical results. It is also possible to predict the value of k_{ij} using models such as the predictive-Peng Robinson or the Enhanced-Predictive-Peng-Robinson-78 equation of state [13]. However, predictive models will not be used in this study since experimental data is available for all the mixtures involved.

Di Marcoberardinoa et al. [14] compared the cycle performance of a CO_2/C_6F_6 mixture using five different EoS. The choice of EoS resulted in an inconsistent cycle thermal efficiency which ranged from 40.5% to 42.5%. They also noted that the choice of the EoS slightly effects the identification of the optimal dopant molar fraction. In the same study, they varied k_{ij} by +/-50% and found that it had a limited effect on the cycle efficiency (+/-0.2%). However, they did not study the effect of k_{ij} on equipment sizing, nor did they investigate its influence in other mixtures.

Previous studies have indicated that thermodynamic property prediction is most consistent near the turbine operating conditions [12], [14]. Therefore, it follows that the turbine should be the component least affected by the fluid model. However, it has not yet been shown to what extent any small variation will impact the final turbine geometry or performance predictions. Answering this question will help with future design efforts by guiding the most suitable choice for the EoS to be used during the mean-line design and numerical computational-fluid dynamic simulation of the turbine, which is a critical component of the cycle.

The aim of the current work is to investigate the sensitivity of key cycle and turbine design parameters to the choice of EoS and k_{ij}uncertainty within a simple recuperated transcritical cycle layout using CO_2-based mixtures as working fluids. Ultimately, the aim is to quantify the effect of EoS and k_{ij} on turbine design. A large scale 100 MWe CSP power plant is considered as a test case because it is the target scale of the SCARABEUS project [15].

METHODOLOGY

Working fluid modelling

This work is part of a research effort that aims to explore the use of CO_2-based working fluids in CSP plants. Therefore, the choice of dopants is focused on those that increase the critical temperature of CO_2 to enable the operation of transcritical cycles in CSP plants. Although the list of chemical compounds is virtually endless, the choice of dopant can be focused by a set of desirable dopant properties: (1) critical temperature above 70 ℃; (2) thermal stability above 700 ℃; and (3) solubility in CO_2 in all cycle conditions. The minimum critical temperature is set to ensure compression occurs far enough from the critical point that the liquid's properties are not drastically affected by small changes in temperature. A critical temperature of 70 ℃ is a safe

distance away from the design pump inlet temperature of 52 ℃ that liquid compression is ensured.

Based on the above criteria, the chosen dopants are: H_2S, C_6F_6, and an unnamed Non-Organic Dopant (NOD). The latter dopant will not be named as it remains confidential within the project consortium. The former two of these dopants have been considered for CO_2 power cycles in previous publications [14], [17]. The main dopant thermophysical parameters of interest are shown in Table 1.

Table 1. Select properties of CO_2 and dopants

Compound	Molecular Weight (g/mol)	Critical Temperature (K)	Critical Pressure (MPa)
CO_2	44.01	31.0	7.382
H_2S	34.08	100.4	8.963
C_6F_6	186.1	242.8	3.273
NOD	>60	<125	<7.000

To calculate the thermophysical properties of the working fluids the thermodynamic models available within Simulis Thermodynamics were used [18]. Validation details were described in the authors' earlier work [19].

The four candidate EoS that were selected for the study are shown in Table 2. The EoS were chosen as to cover three different types: Cubic, Virial, and SAFT. Among these, the cubic types are the most popular owing to their accuracy in the estimation of VLE properties for most fluids. They also require little computational overhead because of their simplicity. However, the accuracy of cubic EoS are limited with highly polar compounds. Although they have the ability to describe mixtures accurately, the application of virial type EoS is limited to low and moderate density fluids. SAFT equations of state are known to produce accurate property estimations away from the critical point and are suitable for systems in which the strength of association varies from weak hydrogen bonds to strong covalent bonds. However, their accuracy comes at a high computational cost.

Table 2. Equations of State used to model the mixtures.

Equation of State	Type	Reference
Peng-Robinson (PR)	Cubic	[20]
Benedict-Webb-Rubbin modified Starling-Nishiumi (BWRS)	Virial	[21]
Soave-Redlich-Kwong (SRK)	Cubic	[22]
Peturbed Chain Statistical Associating Fluid Theory (PC-SAFT)	SAFT	[23]

The cubic EoS requires the definition of the following fluid-specific parameters: acentric factor, critical temperature, and critical pressure. In addition to the parameters required to solve a cubic EoS, the PC-SAFT model requires the following parameters for each pure component of the mixture: (i) the characteristic segment number m, (ii) the characteristic segment size parameter σ, and (iii) the characteristic segment energy parameter ε/k. These parameters are listed in Table 3.

Table 3. SAFT parameters for the pure components

Dopant	m	σ (Å)	ε/k (K)	Reference
CO_2	1.8464	2.98388	140.00	Simulis preset
NOD	>2	>2	>200	Undisclosed
H_2S	1.6686	3.0349	229	[24]
C_6F_6	3.779	3.396	221.65	[14]

Along with the EoS, a k_{ij} value must be specified for each mixture. In this study, k_{ij} was calculated against regressed Vapor-Liquid Equilibrium (VLE) experimental data and used to tune the mixing models for each mixture and EoS pair. Determining the value of k_{ij} required an optimisation problem. By tuning k_{ij}, the calculated VLE lines were manipulated and compared with experimental data to find the best-fit k_{ij} value. An unconstrained gradient-based optimisation approach was used. The weighted least mean square method was used as the objective function. Like the simple least square method, it minimises the residuals between experimental and calculated data, but it also weighs each residual with the experimental uncertainty of the experimental data. The objective function is reduced or expanded depending on the availability of experimental data. The objective function for the optimisation is defined as:

$$f(k_{ij}) = \frac{1}{n_e}\sum_{i=1}^{n_e}\left[\left(\frac{\hat{x}_{1,i}-\tilde{x}_{1,i}}{u^e_{x_{1,i}}}\right)+\left(\frac{\hat{y}_{1,i}-\tilde{y}_{1,i}}{u^e_{y_{1,i}}}\right)+\left(\frac{\hat{T}_i-\tilde{T}_i}{u^e_{T_i}}\right)+\left(\frac{\hat{P}_i-\tilde{P}_i}{u^e_{P_i}}\right)\right] \quad \text{Eq. 1}$$

Where T is the temperature, P is the pressure, and x and y are the liquid and vapour molar fractions of CO_2, respectively. The accents ($\hat{}$) and ($\sim$) indicate the measured and calculated values, respectively. Experimental uncertainty is represented by the term u^{e}. The number of experiments is denoted by n_{e}.

The Mean Absolute Percentage Error (MAPE) is a measure of the accuracy of the thermodynamic model. The lower it is, the more accurate is the model. The MAPE is calculated as follows:

$$MAPE = \frac{100\%}{n_e}\sum_{i=1}^{n_e}\left|\frac{\widetilde{U}_i - \widehat{U}_i}{\widetilde{U}_i}\right| \qquad \text{Eq. 2}$$

where U corresponds to either the temperature or pressure. The MAPE may be used to compare the accuracy of the models to determine their suitability. Based on the MAPE values presented in Table 4, the two cubic equations of state (PR and SRK) are more suitable than the virial equation of state (BWRS) for all mixtures.

Table 4. Binary interaction coefficient and its associated MAPE for each CO_2-based mixture and EoS combination

	Binary Interaction Parameter (k_{ij})			
	PR	**BWRS**	**SRK**	**PC-SAFT**
NOD	0.0214	0.0182	0.0249	-0.0939
C_6F_6	0.0332	0.0626	0.0394	-0.0571
H_2S	0.0871	0.0453	0.0871	-0.0393
	Mean Absolute Percentage Error (MAPE %)			
	PR	**BWRS**	**SRK**	**PC-SAFT**
NOD	2.089	1.938	2.068	4.722
C_6F_6	2.619	5.028	2.374	2.227
H_2S	0.3862	0.4901	0.4025	0.275
	No. of exp. pts		**Source of data**	
NOD	48		Undisclosed	
C_6F_6	64		[25]	
H_2S	122		[26]	

The increase in k_{ij} fidelity with the availability of experimental data is noticeable from Table 4. Among the three mixtures, the experimental data for CO_2/H_2S is the most abundant, thus it has the lowest MAPE in property estimation.

Since the uncertainty in k_{ij} depends on the available VLE data, each mixture has a different range of uncertainty. However, to properly compare the influence of k_{ij} uncertainty in each mixture, a uniform uncertainty of $\pm 50\%$ is applied to all k_{ij} estimates. This negates the effect of VLE data availability when comparing mixtures, which can always be collected through experiments to narrow the uncertainty margins and improve model fidelity.

Thermodynamic cycle model

A simple recuperated tCO_2 cycle is suitable for the purposes of this study because it is a viable option for CSP applications with CO_2-based mixtures. A schematic of the tCO_2 cycle and its Temperature–Entropy diagram are shown in Figure 1.

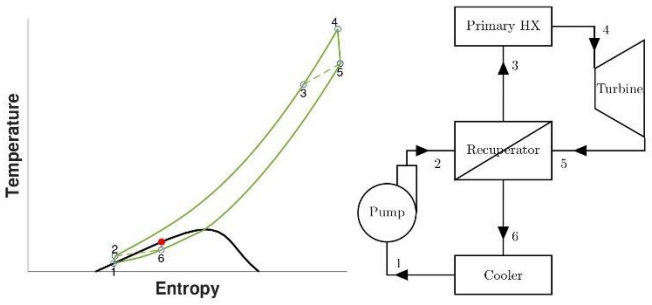

Figure 1. Temperature-Entropy diagram and cycle layout of a simple recuperated tCO_2 cycle operating with a CO_2/C_6F_6 mixture.

The cycle is modelled by applying the first law of thermodynamics to all equipment. Cycle thermal efficiency is expressed as the ratio of the net work produced to the heat consumed by the cycle in Eq.3:

$$\eta_o = \frac{w_n}{q_H} \qquad \text{Eq. 3}$$

The losses within the pump and turbine are approximated by assuming isentropic efficiencies for each component, as expressed by Eq.4 and Eq.5:

$$\eta_p = \frac{h_2 - h_1}{h_2 - h_{1s}} \qquad \text{Eq. 4}$$

$$\eta_t = \frac{h_4 - h_5}{h_4 - h_{5s}} \qquad \text{Eq. 5}$$

where the subscript 's' denotes the outlet conditions assuming isentropic compression and expansion.

The recuperator effectiveness determines the ratio of the actual heat load to the maximum attainable heat load from the stream with the lowest heat-capacity rate, as expressed in Eq.13:

$$\epsilon = \frac{h_5 - h_6}{min\left[\left(h_{T5,P3} - h_{T2,P2}\right), \left(h_{T5,P5} - h_{T2,P6}\right)\right]} \qquad \text{Eq. 6}$$

The cycle state points are determined by setting the pump inlet temperature (T_1), the turbine inlet temperature (T_4), pressure ratio, component efficiencies, and pressure drops. Within this study, T_1 and T_4 will be set according to the values expected in state-of-the-art dry-cooled CSP plants.

Turbine model

For a large 100 MW turbine, a multi-stage axial architecture is recommended [27]. A 1-D mean line turbine design approach was used to model the turbine. The main parameters used to inform turbine design are shown in Eq. 7 to Eq. 9. The blade-loading coefficient (ψ), turbine flow coefficient (ϕ), and degree of reaction (Λ) control the blade speed, fluid axial velocity, and the expansion in the stator and rotor:

$$\psi = \frac{\Delta h_{oi}}{{U_i}^2} \quad \text{Eq. 7}$$

$$\phi = \frac{C_{ai}}{U_i} \quad \text{Eq. 8}$$

$$\Lambda = \frac{\Delta h_{ri}}{\Delta h_{0i}} \quad \text{Eq. 9}$$

where Δh_{oi} is the total enthalpy drop across the stage, U_i is the blade speed of the rotor at the mean radius, C_{ai} is the axial flow velocity at the rotor outlet of the stage, and Δh_{ri} is the enthalpy drop across the rotor. Further details on this design approach are reported in Salah et al. [28]. The number of stages is based on preliminary stress calculations of a previous publication [19].

The specific speed in Eq. 10 is a ratio used to indicate a turbine's size and shape [29].

$$N_s = \frac{N\dot{V}_5^{\frac{1}{2}}}{\Delta h_{oi}^{\frac{3}{4}}} \quad \text{Eq. 10}$$

where N_s and N are the specific speed and nominal speed, respectively. The volume flow rate out of the turbine is represented by $\dot{V}_5$ (in m^3/s).

Optimisation program

A MATLAB program was developed to study the effect of the EoS and k_{ij} on optimal cycle and turbine design. The flowchart in Fig A.1 illustrates the calculation processes for a single CO_2 mixture. The flowchart shows four layers, three of which are parametric studies which change the EoS, k_{ij}, and dopant molar fraction. The inner most layer identifies the optimal cycle condition for the given EoS, k_{ij}, and dopant molar fraction combination. Once optimum cycle conditions are found, the program then produces a turbine geometry using the turbine boundary conditions resulting from the optimal cycle.

Cycle conditions are chosen to simulate those of a CSP plant with dry cooling. Assuming an ambient dry-bulb temperature of 40 ℃ and a minimum temperature difference of 10 ℃ in the condenser, the pump inlet temperature (T_1) is fixed to 50 ℃. Liquid flow into the pump is assumed to be subcooled by 2 ℃ below the saturation pressure. Therefore, the pump inlet pressure (P_1) is set equal to the saturation pressure at 52 ℃. The turbine inlet temperature (T_4) is fixed to 700 ℃, which is the targeted temperature of advanced CSP receiver employing sodium salt as its Heat Transfer Medium (HTM). Finally, the turbine inlet pressure (P_4) is limited to 25 MPa as recommended by Dostal et al. [30]. The turbine design parameters were set based on authors experience. Both the cycle and turbine design inputs are shown in Table 5 and Table 6, respectively.

Table 5. Inputs required for cycle solution

Fixed Parameters			
Parameter		**Range**	**Unit**
Dopant Molar Fraction	X_f	Max(65)	%
Turbine inlet temperature	T_4	700	℃
Pump inlet temperature	T_1	50	℃
Pump efficiency	η_p	85	%
Turbine efficiency	η_t	90	%
Generator efficiency	η_G	99	%
Net electrical power	$\dot{W}_n$	100	MW
Pressure drop primary heat exchanger	$\Delta p/p$	0.015	-
Pressure drop in recuperator high and low-pressure sides	$\Delta p/p$	0.01 and 0.015	-
Pressure drop in condenser	$\Delta p/p$	0.02	-
Dependant Parameters			
Pump inlet pressure	P_1	$P_{sat@T_1+2}$	MPa
Turbine inlet pressure	P_4	Max (25)	MPa
Optimised Parameters			
Pressure Ratio (PR)	r	2 – 4	-
Recuperator Effectiveness	ϵ	70 – 98	%

Table 6. Inputs required for turbine design

Parameter		**Value**	**Unit**
Rotational speed		3000	RPM
Number of stages		4	-
Turbine efficiency	η_t	90	%
Loading coefficient	ψ	1.65	-
Flow coefficient	ϕ	0.23	-
Degree of reaction	Λ	0.5	-

RESULTS AND DISCUSSION

Attention is first given to the choice of the optimal dopant molar fraction. This is important because it defines all subsequent fluid properties. In essence, a variation in the dopant molar fraction of

a mixture produces different fluids. As seen in Figure 2, the thermal efficiency of the cycle is affected by the dopant molar fraction, the EoS, and the value of k_{ij}, but this effect differs depending on the mixture. Generally, thermal efficiency fluctuates around $\pm 0.1\%$ to $\pm 0.3\%$ of the baseline value for both variations in the EoS and k_{ij}. The largest variation due to k_{ij} is 0.7% and it is observed in BWRS when used with CO_2/C_6F_6. Among the four EoS, the two cubic EoS, PR and SRK, are the least sensitive to variations in k_{ij}. This is confirmed by the averaged MAPE values shown in the Figure 2 for each combination. The MAPE was calculated by comparing the results obtained with k_{ij} variations against the baseline of no variation in k_{ij}.

Moreover, the cycle thermal efficiency for all mixtures and EoS shows a positive correlation with k_{ij}, where higher values of k_{ij} produce cycles of higher thermal efficiencies. Also common among mixtures is that the thermal efficiency exhibits the same trend with dopant fraction regardless of the EoS or k_{ij}, which suggests that the dopant fraction that yields the highest thermal efficiency is independent of the fluid model used. This is further confirmed through Figure 3, which shows that neither EoS nor k_{ij} affect the choice of the optimal dopant fraction. Furthermore, during the optimisation it was found that all optimal cycles lead to the maximum permissible pressure at turbine inlet (i.e., 25 MPa).

Taking a closer look at the thermal efficiency for the same optimal dopant fractions reveals some differences in the prediction of cycle performance. Figure 4 shows the maximum percentage difference resulting from the choice of the EoS and the variation in k_{ij}. The maximum percentage difference between the EoS was calculated based on the difference between the EoS that yields the lowest efficiency and the EoS that yields the highest. The maximum percentage difference resulting from k_{ij} variation was calculated by comparing the efficiency change due to k_{ij} variation with the baseline case of no k_{ij} variation.

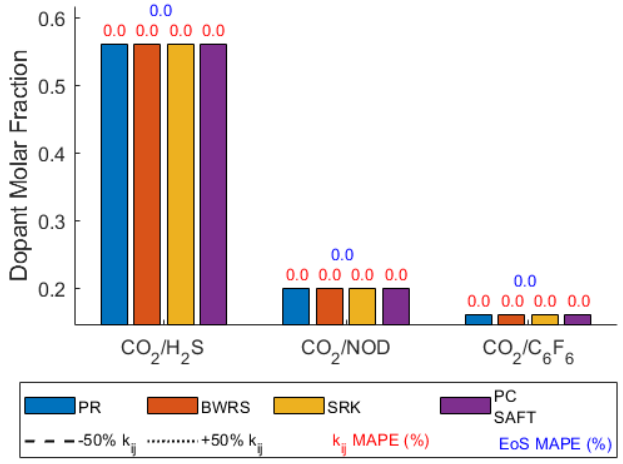

Figure 3. Effect of choice of EoS and variation in k_{ij} on the optimal dopant molar fraction.

As observed from Figure 4, different mixtures respond differently to the EoS. Cycles operating with CO_2/C_6F_6 are affected the most, with a maximum percentage change of 2.3%, which equates to a 1% nominal change in efficiency between SRK and PC-SAFT. The other two dopants are affected half as

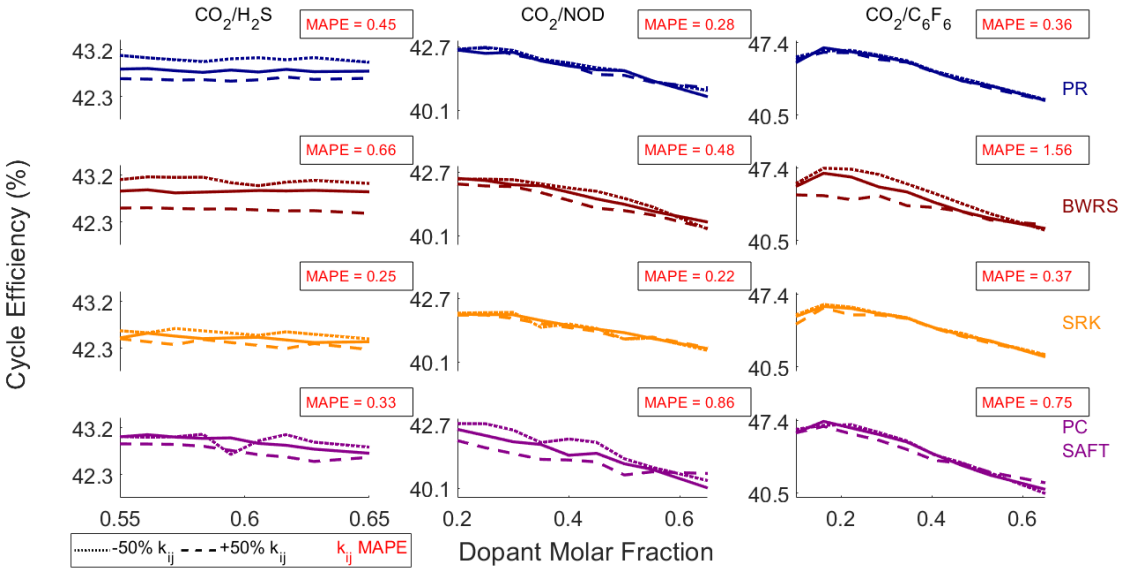

Figure 2. The effect of dopant molar fraction on cycle thermal efficiency depending on the choice of EoS and the variation in k_{ij}.

much. Overall, the effect of k_{ij} variation is less pronounced, except when modelling a CO_2/C_6F_6 mixture using the BWRS EoS where a decrease in the value of k_{ij} results in cycle efficiency estimates lower by more than 2% nominal efficiency (i.e. 44.77% compared to 46.90%).

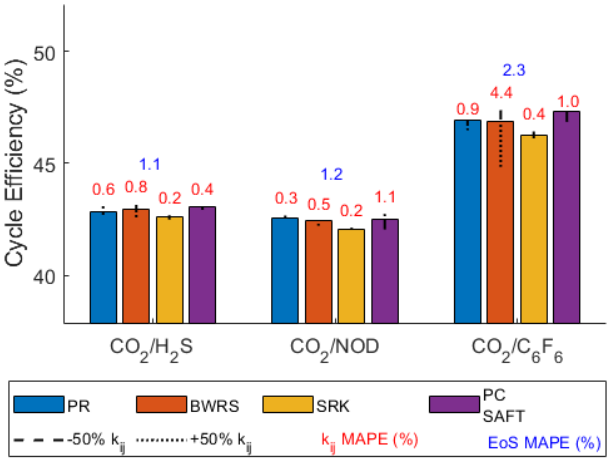

Figure 4. Effect of choice of EoS and variation in k_{ij} on cycle thermal efficiency.

Before investigating the effect on turbine design, the change in pump design will be addressed. Because of real-gas effects any deviation in the EoS leads to a larger variation in properties near the saturation region. This variation is apparent in the design point parameters of the pump, indicated by the differential head and volume flow rate. As observed in Figure 5, both head and flow rate change with EoS and k_{ij}. For all cases, the change in flow rate is greater than the change in head. In the most extreme case, the SRK predicts almost twice the flow rate for CO_2/H_2S and CO_2/C_6F_6 than the PC-SAFT does. Consequently, half as many pumps may be predicted to be required if the PC-SAFT EoS is used to model the cycle. The change in head and flow rate is also significant due to k_{ij} variation. The maximum change in flow rate and pump head is 34.2% and 14.7%, respectively, if the BWRS is used to model CO_2/C_6F_6. These findings agree with previous studies which identified the significant influence of the fluid model on the pump in particular.

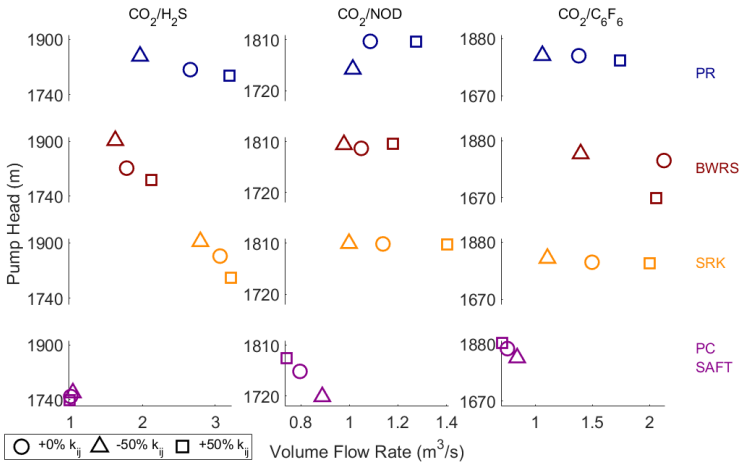

Figure 5. Effect of choice of EoS and variation in k_{ij} on the pump specific speed.

As seen in the following figures, the fluid properties at turbine inlet are less affected by the change in the fluid model than the properties at pump inlet. This is partly because of the aforementioned real gas effects at pump inlet, but also because

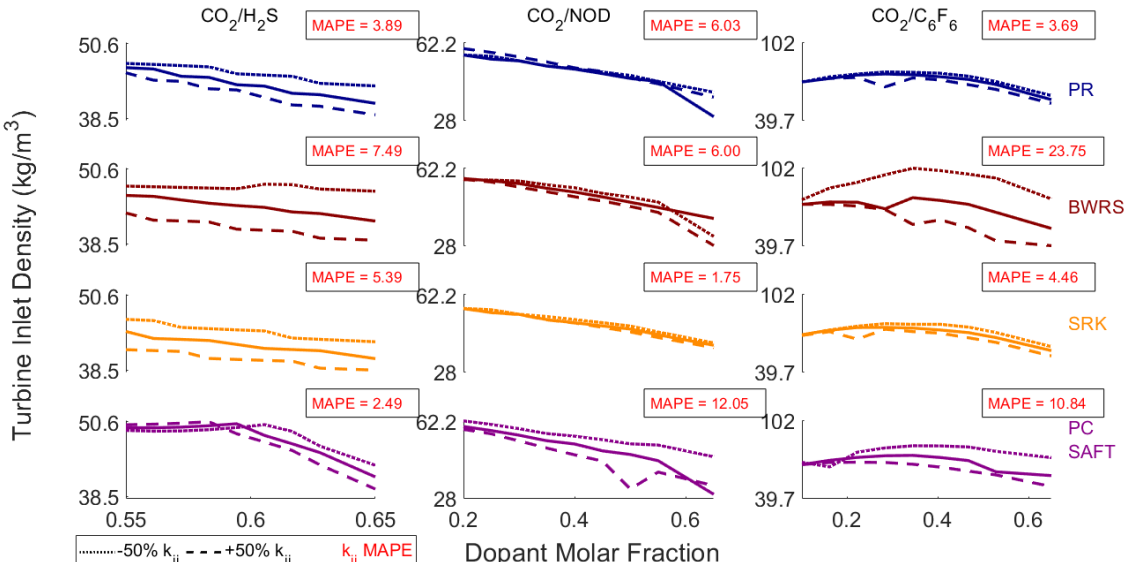

Figure 6 The effect of dopant molar fraction on the fluid's density at turbine inlet depending on the choice of EoS and the variation in k_{ij}.

the turbine inlet conditions are identical for all cases (700 ℃ and 25 MPa), while the pump inlet pressure varies depending on the EoS and k_{ij}. However, there is an observable variation in turbine inlet density, as shown in Figure 6. The maximum MAPE between the baseline models of the EoS are 8.3%, 2.4%, and 4.5% for H_2S, NOD, and C_6F_6 mixtures, respectively. Therefore, the turbine inlet density of cycles operating with CO_2/NOD is generally less sensitive than those operating with the other two. Moreover, The variation in density for the optimal blend fraction, described in Figure 7, is less severe than the general trend shown in Figure 6, yet the MAPE is still the highest for CO_2/C_6F_6.

Similar to the trend observed in pump design variation, the two cubic EoS exhibit the lowest sensitivity to k_{ij} variation even away from the critical point. This consistency suggests that cubic EoS are more robust and may be a good option in the absence of quality experimental data from which k_{ij} can be calibrated. Among the four EoS, the BWRS is the most sensitive to k_{ij} variation, therefore precise k_{ij} values are recommended when employing the BWRS EoS.

The density of the fluid directly affects the expansion work of the turbine. Therefore, its variation is reflected in the variation in the turbine specific work. As seen in Figure 8 and Figure 9, the trend in specific work variation is similar to that in density, but in the opposite direction. Turbine loading, mechanical stresses, and number of stages are partly determined by the specific work, since the specific work is related to blade speed through the loading coefficient and the blade speed is constrained based on mechanical design constraints. A difference of 13.7% in density like that observed between SRK and PC-SAFT for CO_2/H_2S could produce slightly different turbine designs, as seen later.

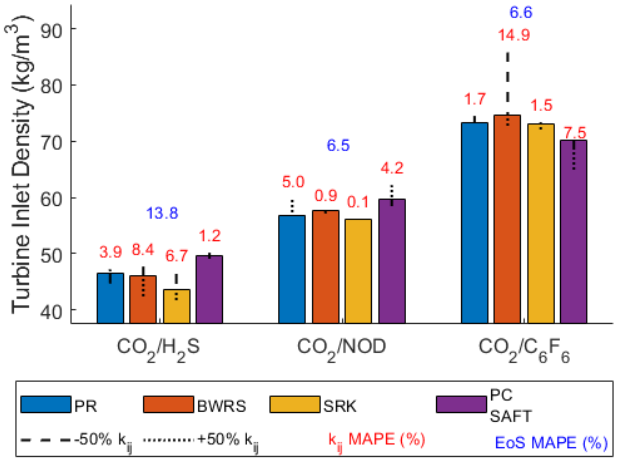

Figure 7 Effect of choice of EoS and variation in k_{ij} on the density of the fluid at turbine inlet.

The implications of density dissimilarity and the subsequent dissimilarity in turbine specific work are reflected in the specific speed of the turbine, shown in Figure 10. The specific speed was calculated for the entire turbine (across the four stages) by substituting the total enthalpy drop across the turbine in Eq.10. Although the percentage change is considerable for some cases, such as 21% for BWRS with CO_2/C_6F_6, the nominal change in specific speed is miniscule; no larger than 0.3 rad/s for the same case. This indicates that the resulting turbine designs will be comparable in shape and size for all EoS and k_{ij} values.

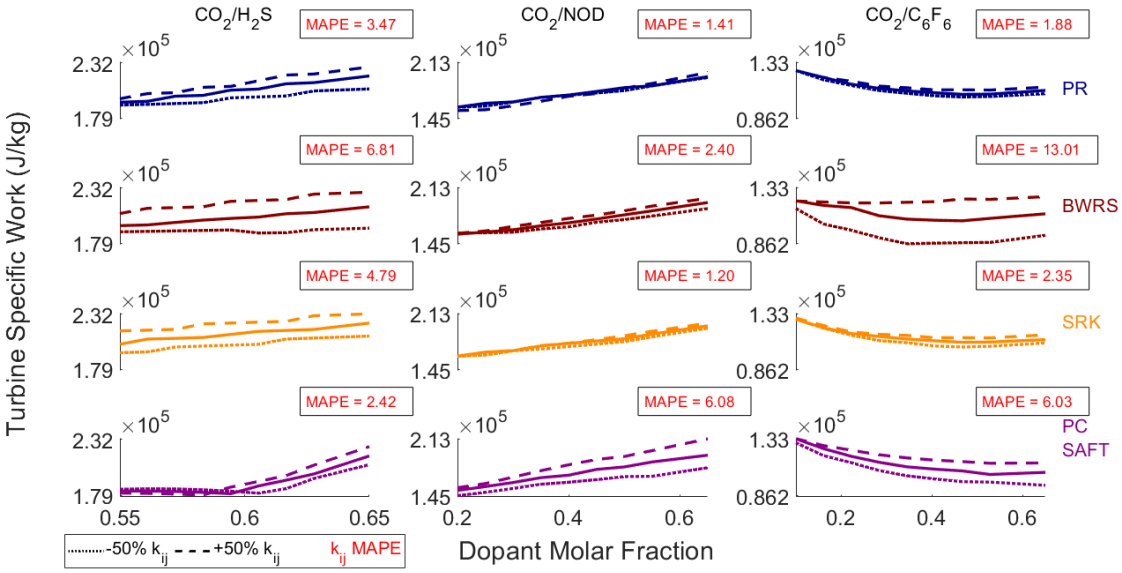

Figure 8 The effect of dopant molar fraction on the turbine specific work depending on the choice of EoS and the variation in k_{ij}.

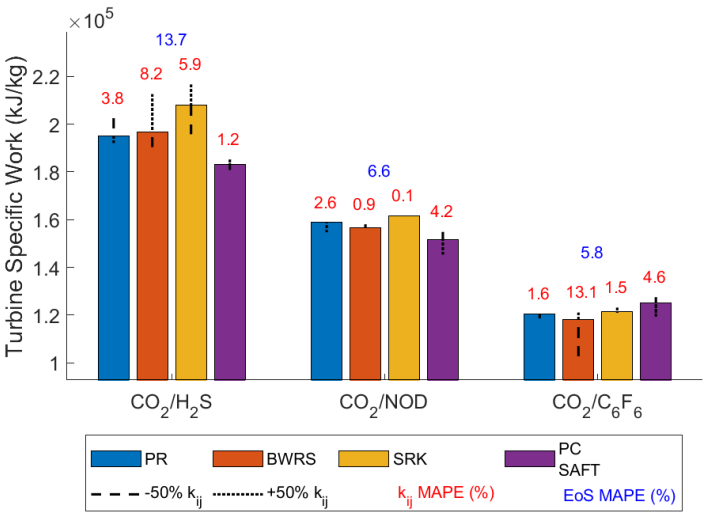

Figure 9 Effect of choice of EoS and variation in k_{ij} on the turbine specific work

The changes in turbine design parameters culminate in the resulting turbine geometry represented by its mean diameter and blade height. The turbine mean diameter is measured at the meridional profile midspan of the turbine blades and is assumed to be constant across all turbine stages. The meridional blade profile of the turbine geometry corresponding to the optimal dopant fraction for each mixture, EoS, and k_{ij} variation combinations are presented in Figure 11. Consistent with the trends observed in the previous figures, the effect of EoS is more pronounced in CO_2/H_2S mixtures. The largest difference is between SRK and PC-SAFT, which amounts to 6.3% (6.6 cm) difference in the mean diameter and a 18.8% (1.04 cm) difference in the blade height at the final stage. The EoS effects the other two mixtures half as much.

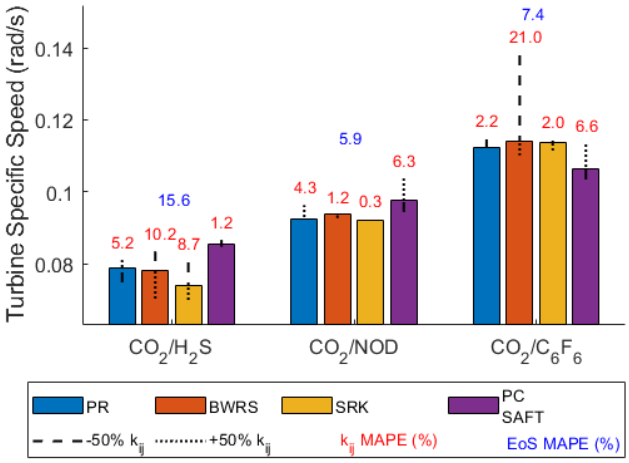

Figure 10 Effect of choice of EoS and variation in k_{ij} on the turbine specific speed

The effect of k_{ij} variation on turbine geometry is smaller than that of the EoS, except in the case of BWRS with CO_2/C_6F_6 which yields a difference of 6.7% (5.6 cm) in mean diameter and 27.3% (2.73 cm) in blade height of the last stage when k_{ij} is set to 0.5 of its baseline values. The mixture and EoS combinations that are practically insensitive to k_{ij} variations are: CO_2/H_2S with PC-SAFT, CO_2/NOD with BWRS or SRK, and CO_2/C_6F_6 with PR or SRK. Moreover, the PR EoS with CO_2/H_2S or CO_2/NOD mixtures or PC-SAFT with CO_2/C_6F_6 are also

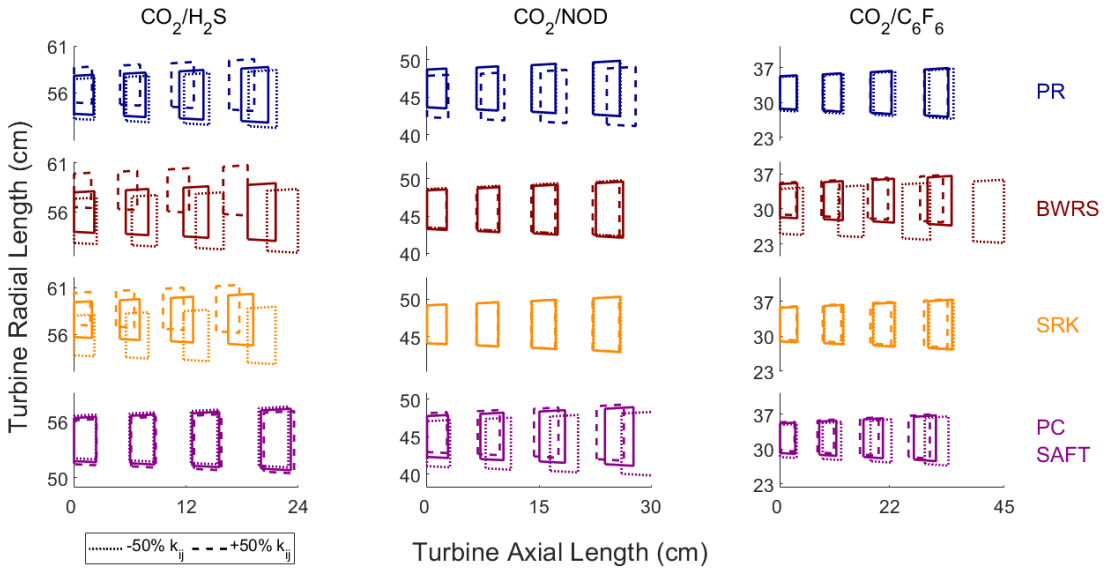

Figure 11 The meridional flow path for the four-stage turbine corresponding to the optimal dopant fractions.

relatively insensitive to k_{ij} variations as they exhibit only small variations. Even though the turbine geometry is affected by fluid model variations, that effect does not change the turbine design fundamentally as seen in Figure 11. The same was revealed through the small change in turbine specific speed.

The Mach number of a fluid is important to determine whether subsonic or supersonic flow is present. By assuming similar velocities for all cases, the Mach number may be compared by comparing the speed of sound at turbine inlet. As shown in Figure 12, the speed of sound remains fairly constant regardless of the fluid model. The MAPE due to k_{ij} variation for all EoS and mixture combinations were less than 0.2%. Moreover, the MAPE due to EoS selection is 2.0% at its highest for CO_2/C_6F_6. Overall, it seems that Mach number prediction will unlikely to be affected by the fluid model.

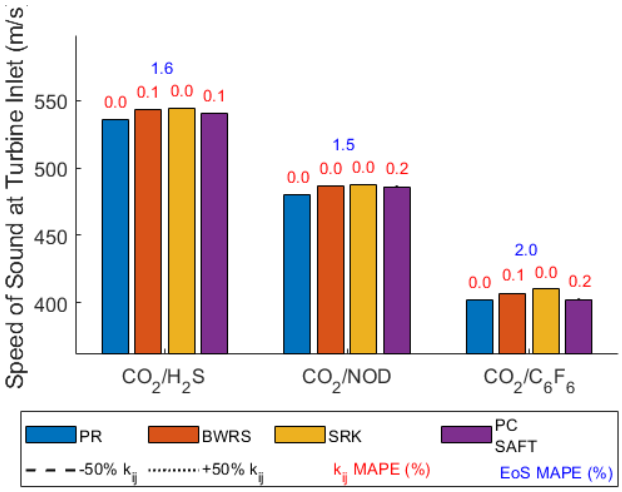

Figure 12 Effect of choice of EoS and variation in k_{ij} on the speed of sound at turbine inlet.

CONCLUSION

In this paper, the sensitivity of cycle and turbine design to the fluid property model was investigated. The study included three CO_2-based mixtures (CO_2/H_2S, CO_2/NOD, and CO_2/C_6F_6) in combination with four equations of state (PR, BWRS, SRK, and PC-SAFT), each modelled under scenarios of k_{ij} uncertainty ($\pm$50%).

It was found that the choice of the dopant fraction which yields maximum cycle thermal efficiency for each mixture is independent from the fluid model used. However, the predicted optimal thermal efficiency of the mixtures is reliant on the fluid model. Absolute thermal efficiency may vary by a maximum of 1% due to the choice of the EoS when modelling CO_2/C_6F_6, and by up to 2% due to k_{ij} uncertainty when the BWRS EoS is used to model CO_2/C_6F_6. Moreover, cycle thermal efficiency was observed to have a positive correlation with the k_{ij} value for all mixture and EoS combinations.

In terms of turbine design, among the three mixtures, CO_2/NOD is the least sensitive to the fluid model, while the other two are nearly equally sensitive. Furthermore, the two cubic equations of state, PR and SRK, are generally less sensitive to k_{ij} variation the other two EoS, except for the case of CO_2/H_2S. This suggests that they offer more robust property prediction in the absence of quality experimental data. On the other hand, the BWRS EoS is especially sensitive to k_{ij} uncertainty, thus requires precise model calibration before it can be used reliably. Lastly, the maximum difference in the turbine geometry due to the choice of the EoS amounted to 6.3% (6.6 cm) difference in the mean diameter and a 18.8% (1.04 cm) difference in the blade height at the final stage. On the other hand, the maximum difference in turbine geometry as a result of k_{ij} uncertainty amounted to 6.7% (5.6 cm) in mean diameter and 27.3% (2.73 cm) in blade height of the last stage.

NOMENCLATURE

Acronyms	
BWRS	Benedict-Webb-Rubin-Starling
CSP	Concentrated Solar Power
EoS	Equation of State
HTM	Heat Transfer Medium
MAPE	Mean Absolute Percentage Error
MITA	Minimum Internal Temperature Approach
PC-SAFT	Perturbed Chain Statistical Associating Fluid Theory
PR	Peng-Robinson
sCO_2	Supercritical Carbon Dixoide
SRK	Soave-Redlich-Kwong
tCO_2	Transcritical Carbon Dioxide
VLE	Vapor-Liquid Equilibrium
Symbols	
η	Efficiency
ϵ	Effectiveness
k_{ij}	Binary interaction coefficient
ψ	Loading coefficient
ϕ	Flow coefficient
Λ	Degree of reaction
h	Specific enthalpy, J/kg
ρ	Density, kg/m^3
H	Head, m
N	Rotational speed, RPM
P	Pressure, MPa
r	Pressure ratio

T	Temperature, ℃

ACKNOWLEDGEMENTS

This project has received funding from the European Union's Horizon 2020 research and innovation programme under grant agreement No. 814985.

REFERENCES

[1] S. Polimeni, M. Binotti, L. Moretti, and G. Manzolini, "Comparison of sodium and KCl-MgCl2 as heat transfer fluids in CSP solar tower with sCO2 power cycles," *Sol. Energy*, vol. 162, pp. 510–524, Mar. 2018.

[2] K. Wang, Y. L. He, and H. H. Zhu, "Integration between supercritical CO2 Brayton cycles and molten salt solar power towers: A review and a comprehensive comparison of different cycle layouts," *Appl. Energy*, vol. 195, pp. 819–836, 2017.

[3] T. Neises and C. Turchi, "A comparison of supercritical carbon dioxide power cycle configurations with an emphasis on CSP applications," in *Energy Procedia*, 2014, vol. 49, pp. 1187–1196.

[4] M. Atif and F. A. Al-Sulaiman, "Energy and exergy analyses of solar tower power plant driven supercritical carbon dioxide recompression cycles for six different locations," *Renewable and Sustainable Energy Reviews*, vol. 68. Elsevier Ltd, pp. 153–167, 01-Feb-2017.

[5] M. Cerio Vera, "S-CO2 for efficient power generation with energy storage," 2015.

[6] J. D. Osorio, R. Hovsapian, and J. C. Ordonez, "Effect of multi-tank thermal energy storage, recuperator effectiveness, and solar receiver conductance on the performance of a concentrated solar supercritical CO 2 - based power plant operating under different seasonal conditions," *Energy*, vol. 115, pp. 353–368, Nov. 2016.

[7] T. G. Lewis, T. M. Conboy, and S. A. Wright, "Supercritical CO2 Mixture Behavior for Advanced Power Cycles and Applications," 2011.

[8] J. Xia, J. Wang, G. Zhang, J. Lou, P. Zhao, and Y. Dai, "Thermo-economic analysis and comparative study of transcritical power cycles using CO2-based mixtures as working fluids," *Appl. Therm. Eng.*, vol. 144, pp. 31–44, Nov. 2018.

[9] C. M. Invernizzi and T. Van Der Stelt, "Supercritical and real gas Brayton cycles operating with mixtures of carbon dioxide and hydrocarbons," *Proc. Inst. Mech. Eng. Part A J. Power Energy*, vol. 226, no. 5, pp. 682–693, Aug. 2012.

[10] D. Bonalumi, S. Lasala, and E. Macchi, "CO2-TiCl4 working fluid for high-temperature heat source power cycles and solar application," *Renew. Energy*, 2018.

[11] G. Manzolini, M. Binotti, D. Bonalumi, C. Invernizzi, and P. Iora, "CO 2 mixtures as innovative working fluid in power cycles applied to solar plants. Techno-economic assessment," *Sol. Energy*, vol. 181, no. June 2018, pp. 530–544, 2019.

[12] Q. Zhao, M. Mecheri, T. Neveux, R. Privat, and J. N. Jaubert, "Selection of a Proper Equation of State for the Modeling of a Supercritical CO2 Brayton Cycle: Consequences on the Process Design," *Ind. Eng. Chem. Res.*, vol. 56, no. 23, pp. 6841–6853, 2017.

[13] S. Lasala, A.-P. Martinez, and J.-N. Jaubert, "A Predictive Equation of State to Perform an Extending Screening of Working Fluids for Power and Refrigeration Cycles," in *Organic Rankine Cycles for Waste Heat Recovery - Analysis and Applications*, IntechOpen, 2020.

[14] G. Di Marcoberardino, E. Morosini, and G. Manzolini, "Influence of the Equations of state on the performance of CO2 + C6F6 as innovative working fluid in transcritical cycles," Unpublished, 2021.

[15] M. Binotti, G. Di Marcoberardino, P. Iora, and C. Invernizzi, "SCARABEUS : Supercritical carbon dioxide / alternative fluid blends for efficiency upgrade of solar power plants SCARABEUS : Supercritical Carbon Dioxide / Alternative Fluid Blends for Efficiency Upgrade of Solar Power Plants," vol. 130002, no. December, 2020.

[16] SCARABEUS, "SCARABEUS Project," 2019. [Online]. Available: https://www.scarabeusproject.eu/. [Accessed: 13-Nov-2019].

[17] X. Liu, Z. Xu, Y. Xie, and H. Yang, "CO2-based mixture working fluids used for the dry-cooling supercritical Brayton cycle: Thermodynamic evaluation," *Appl. Therm. Eng.*, vol. 162, no. 17923, p. 114226, 2019.

[18] ProSim, "Simulis Thermodynamics," 2019. [Online]. Available: http://www.prosim.net/en/software-simulis-thermodynamics-mixture-properties-and-fluid-phase-equilibria-calculations-3.php. [Accessed: 13-Nov-2019].

[19] O. Aqel, M. White, M. Khader, and A. Sayma, "Sensitivity of transcritical cycle and turbine design to dopant fraction in CO2-based working fluids," *Appl. Therm. Eng.*, 2021.

[20] D. Y. Peng and D. B. Robinson, "A New Two-Constant Equation of State," *Ind. Eng. Chem. Fundam.*, vol. 15, no. 1, pp. 59–64, 1976.

[21] H. Nishiumi and S. Saito, "An improved generalized BWR equation of state applicable to low reduced temperatures," *J. Chem. Eng. Japan*, vol. 8, no. 5, pp. 356–360, 1975.

[22] G. Soave, "Equilibrium constants from a modified Redlich-Kwong equation of state," *Chem. Eng. Sci.*, vol. 27, no. 6, pp. 1197–1203, 1972.

[23] J. Gross and G. Sadowski, "Perturbed-chain SAFT: An equation of state based on a perturbation theory for chain molecules," *Ind. Eng. Chem. Res.*, vol. 40, no. 4, pp. 1244–1260, 2001.

[24] A. Yazdi, A. Najafloo, and H. Sakhaeinia, "A method for thermodynamic modeling of H2S solubility using PC-

SAFT equation of state based on a ternary solution of water, methyldiethanolamine and hydrogen sulfide," *J. Mol. Liq.*, vol. 299, 2020.

[25] A. M. A. Dias *et al.*, "Vapor - Liquid equilibrium of carbon dioxide - Perfluoroalkane mixtures: Experimental data and SAFT modeling," *Ind. Eng. Chem. Res.*, vol. 45, no. 7, pp. 2341–2350, 2006.

[26] J. A. Bierlein and W. B. Kay, "Phase-Equilibrium Properties of System Carbon Dioxide-Hydrogen Sulfide," *Ind. Eng. Chem.*, vol. 45, no. 3, pp. 618–624, 1953.

[27] J. J. Sienicki, A. Moisseytsev, R. L. Fuller, S. A. Wright, and P. S. Pickard, "Scale Dependencies of Supercritical Carbon Dioxide Brayton Cycle Technologies and the Optimal Size for a Next-Step Supercritical CO 2 Cycle Demonstration," 2011.

[28] S. I. Salah, M. A. Khader, M. T. White, and A. I. Sayma, "Mean-Line Design of a Supercritical CO 2 Micro Axial Turbine," *Appl. Sci.*, pp. 1–20, 2020.

[29] O. E. Baljé, "A study on design criteria and matching of turbomachines: Part A-similarity relations and design criteria of turbines," *J. Eng. Gas Turbines Power*, vol. 84, no. 1, pp. 83–102, 1962.

[30] V. Dostal, M. J. Driscoll, and P. Hejzlar, "A Supercritical Carbon Dioxide Cycle for Next Generation Nuclear Reactors," 2004.

Appendix A

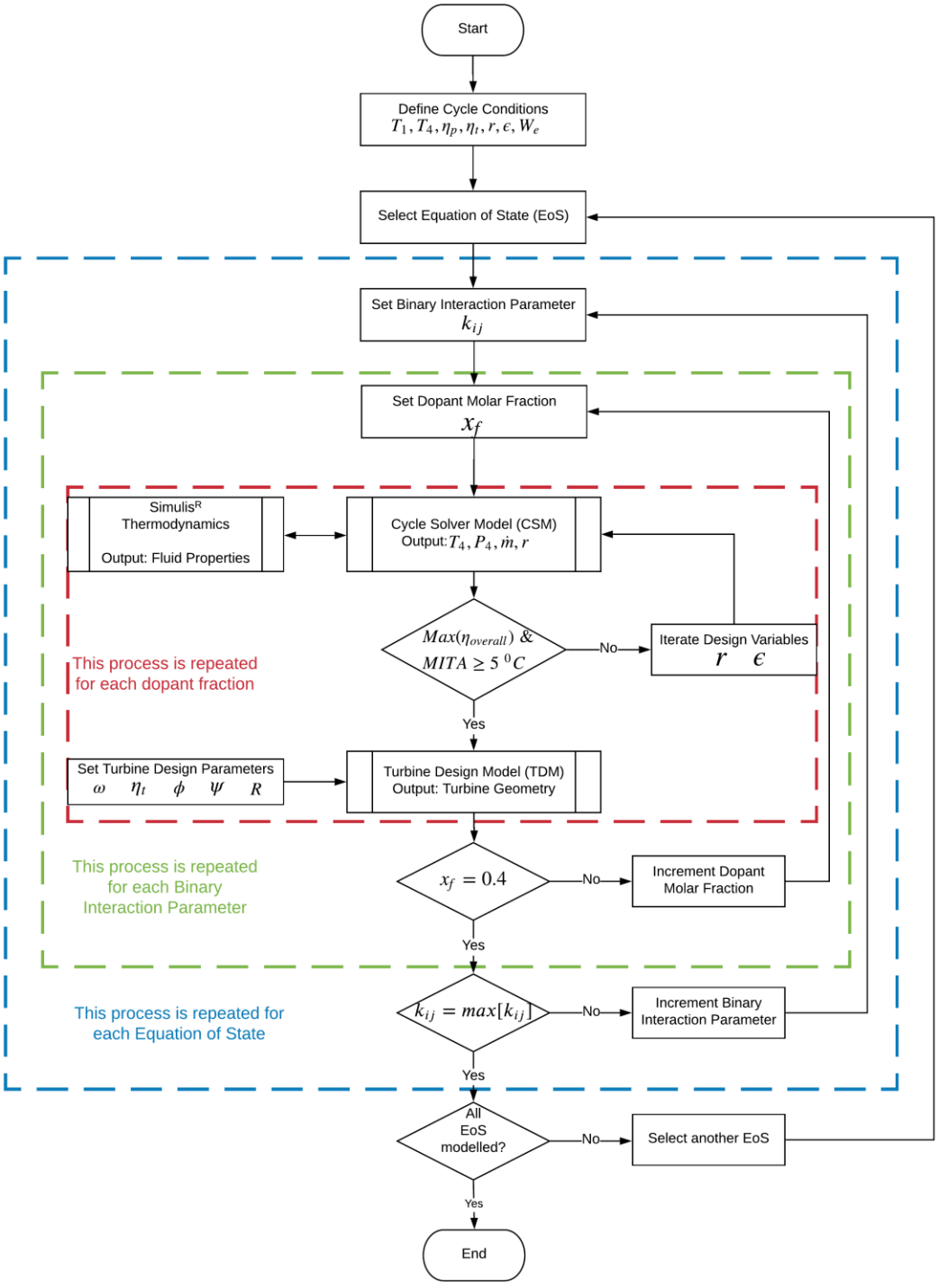

Fig A1. Flowchart of the sensitivity study for a single CO_2 mixture.

DuEPublico

Duisburg-Essen Publications online

UNIVERSITÄT DUISBURG ESSEN

Offen im Denken

ub | universitäts bibliothek

Published in: 4th European sCO2 Conference for Energy Systems, 2021

This text is made available via DuEPublico, the institutional repository of the University of Duisburg-Essen. This version may eventually differ from another version distributed by a commercial publisher.

DOI: 10.17185/duepublico/73959
URN: urn:nbn:de:hbz:464-20210330-104458-0

This work may be used under a Creative Commons Attribution 4.0 License (CC BY 4.0).